Published in final edited form as:
J Cell Physiol. 2009 June ; 219(3): 734–743. doi:10.1002/jcp.21717.

Nmp4/CIZ Suppresses Parathyroid Hormone-Induced Increases in Trabecular Bone

ALEXANDER G. ROBLING[1,2], **PAUL CHILDRESS**[1], **JUN YU**[1], **JESSICA COTTE**[1], **AARON HELLER**[1], **BINU K. PHILIP**[1], and **JOSEPH P. BIDWELL**[1,*]

[1] Department of Anatomy & Cell Biology, Indiana University School of Medicine (IUSM), Indianapolis, Indiana

[2] Department of Biomedical Engineering, Indiana University-Purdue University at Indianapolis, Indiana

Abstract

The nucleocytoplasmic shuttling transcription factor Nmp4/CIZ (nuclear matrix protein 4/cas interacting zinc finger protein) is a ubiquitously expressed protein that regulates both cytoplasmic and nuclear activities. In the nucleus, Nmp4/CIZ represses transcription of genes crucial to osteoblast differentiation and genes activated by various anabolic stimuli, including parathyroid hormone (PTH). We investigated the role of Nmp4/CIZ in the PTH-induced increase in bone by engineering mice with loss-of-function mutations in the Nmp4/CIZ gene, and treating 10-week-old female mice with anabolic doses of human PTH (1–34) at 30 μg/kg/day, 7 day/week, for 7 weeks or vehicle control. The untreated, baseline phenotype of the Nmp4-null mice between 8 and 16 weeks of age included a modest but significant increase in bone mineral density (BMD) and bone mineral content (BMC) compared to wild-type (WT) mice. Type I collagen mRNA expression was moderately elevated in the femurs of the Nmp4-null mice. The Nmp4 mutant alleles decreased body weight by 4% when expressed on a mixed background but the same alleles on a pure B6 background yielded a significant, 15% increase in body weight among the KO mice, compared to their WT controls. Hormone treatment equally enhanced BMD and BMC over vehicle-treated mice in both the WT and Nmp4-null groups but Nmp4-KO mice exhibited a significantly greater PTH-induced acquisition of femoral trabecular bone as compared to WT mice. These data support our hypothesis that Nmp4/CIZ is a transcriptional attenuator that suppresses osteoid synthesis and PTH-mediated acquisition of cancellous bone.

An accumulating body of clinical studies demonstrates that once-daily intermittent doses of human parathyroid hormone (1–34) [hPTH (1–34)] reduce the fracture risk in patients with severe osteoporosis (Dempster et al., 2001; Neer et al., 2001). Despite its proven efficacy in reducing fractures, and subsequent FDA approval as an osteoporosis therapy, the cellular and molecular mechanisms of action employed by intermittent PTH remain to be fully elucidated. Upon binding to its receptor (PTHR1), PTH activates a multitude of osteoblast molecular signaling networks, beginning with the cAMP/PKA and the cytosolic calcium/PKC response limbs. Subsequent downstream targets include the activation of the transcription factors CREB and Runx2, downregulation of the osteocyte-derived bone formation inhibitor sclerostin, and initiation of an IGF-1 autocrine/paracrine signaling loop, among others (Feister et al., 2000; Bikle et al., 2002; Swarthout et al., 2002; Hurley et al., 2006; Yakar et al., 2006; Zhang et al.,

*Correspondence to: Joseph P. Bidwell, Department of Anatomy & Cell Biology, Indiana University School of Medicine (IUSM), Medical Science Bldg 5035, 635 Barnhill Drive, Indianapolis, IN 46202. E-mail: jbidwell@iupui.edu.
Jun Yu's present address is Lilly Corporate Center, Indianapolis, IN 46285.

A. Robling and P. Childress contributed equally to this manuscript.

2006; Leupin et al., 2007; Li et al., 2007; Merciris et al., 2007). The collective end result of these and other PTH-induced networks is the enhanced differentiation of committed osteoblast precursors in the bone marrow, and prolongation of the lifespan of the mature osteoblast via suppressed apoptosis (reviewed in Jilka, 2007; Martin and Seeman, 2007).

While much of the investigation of anabolic PTH signal transduction and molecular regulation has been focused on the activation of osteogenic kinases, secretion of osteogenic ligands and ECMs, and expression of osteogenic genes, little is known about the inhibitory mechanisms on bone formation that are also activated by the anabolic signaling events. These mechanisms, though antagonistic to the bone-building effects of the signal, likely serve as an important negative feedback mechanism to prevent hyper-responsiveness to the signal. For example, the anti-apoptotic effect of PTH on osteoblasts requires Runx2-driven transcription of survival genes but PTH also induces the Smurf1-mediated proteasomal degradation of this trans-acting protein (Bellido et al., 2003). This mechanism appears to support a self-limiting response of the hormone's own anabolic action, though it has not been tested in vivo. Similarly, up-regulation of the CREM gene, the products of which act as transcriptional attenuators, may keep the anabolic response to intermittent PTH in check, by restraining PTH-induced osteoclastogenesis (Liu et al., 2007). Elucidation of the osteo-inhibitory mechanisms that are activated by anabolic PTH could yield an attractive target for osteoporosis therapy, either alone or in conjunction with PTH treatment, by essentially providing a means to suppress the "off signal" that accompanies each anabolic activation cycle.

We have potentially identified such a target in a series of experiments conducted over the last 12 years (Alvarez et al., 1997, 1998, 2005; Thunyakitpisal et al., 2001; Shah et al., 2004). Nuclear matrix protein 4/cas interacting zinc finger protein (Nmp4/CIZ) is a trans-acting nucleocytoplasmic shuttling protein that, in osteoblasts, acts as a transcriptional attenuator (Shen et al., 2002; Shah et al., 2004; Morinobu et al., 2005). Nmp4/CIZ suppresses PTH-driven matrix metalloproteinase-13 (MMP-13) gene transcription in MC3T3-E1 osteoblast-like cells (Shah et al., 2004). Similarly BMP2-induced up-regulation of alkaline phosphatase, osteocalcin, and type I collagen are all suppressed in MC3T3-E1 cells over-expressing Nmp4/CIZ (Shen et al., 2002), and BMP2- induced bone formation on adult calvariae in vivo was enhanced by CIZ deficiency (Morinobu et al., 2005). Collectively, our studies indicate that Nmp4/CIZ activation induced by anabolic regimens of PTH might be a mechanism to partially antagonize the osteogenic response of bone tissue to therapeutic doses of PTH. From these data, an obvious question emerges: does the anabolic response to PTH improve when Nmp4/CIZ is disabled/deleted? If so, Nmp4/CIZ might represent an attractive pharmacologic target for inhibition in the search for new osteoporosis therapies.

In the present communication, we examine the role of Nmp4/CIZ in normal skeletal homeostasis and in regulating the response of the skeleton to intermittent PTH. We engineered mice with a loss-of-function mutation in Nmp4/CIZ, and measured bone mass, density, structure, and gene expression, at several time points. We further evaluated the ramifications of the null mutation on anabolic PTH signaling by challenging the mice with intermittent PTH for 7 weeks. Nmp4-null mice exhibited a modest gain in skeletal BMD and BMC between 8 and 16 weeks of age as compared to WT animals. Notably, the Nmp4-knockout (KO) animals displayed a significantly enhanced hormone-induced gain in femoral cancellous bone. The present data and our previous in vitro studies support our hypothesis that Nmp4/CIZ is a key component to an inhibitory mechanism of bone formation. As such, it appears to act as a transcriptional attenuator that suppresses osteoid synthesis thus limiting anabolic PTH-mediated gains in cancellous bone.

Materials and Methods

Generation of Nmp4-knockout (KO) mice

Construction of targeting vector—Our local Institutional Animal Care and Use Committee (IACUC) approved all experiments and procedures involving the production and use of the experimental mice described in this study. Nmp4-null mice were prepared under our direction at the in Genious Targeting Laboratories, Inc., Stony Brook, NY. The strategy used in preparing these mice involved replacing the region of the Nmp4 gene containing coding exons 4–7 with the Neo gene cassette (see Fig. 1A). Briefly, a 14.5 kb mouse genomic DNA fragment was cloned from the mouse 129Sv/Ev lambda genomic library. This genomic fragment contains exons 4–7 of the mouse *Nmp4* gene. The targeting vector was constructed by using 3 kb DNA fragment as the short arm, which was a PCR fragment from primers NMPYA1 to NMPYA2 (Table 1). Primer NMPYA1 is located 3 kb upstream of exon 1 and primer NMPYA2 is located in exon 1 and 45 bp upstream of the ATG start codon. The short arm was inserted into the 5′ end of the Neo gene cassette using the MluI site. The long arm was an 11 kb genomic fragment that starts from BsrGI site to the end of the lambda clone.

Screening of recombinant clones—Ten micrograms of the targeting vector was linearized by NotI and then transfected by electroporation of iTL1 embryonic stem cells (ES, 129Sv/Ev). After selection in G418 antibiotic, 200 resistant colonies were expanded for PCR analysis to identify recombinant clones. Primers, A1, A2, and A3 (Table 1) were designed upstream 5′ to the short homology arm outside the region used to generate the targeting construct. PCR reactions (94°C 20 sec; 62°C60 sec; 72°C 240 sec; 35 cycles) using A1, A2, or A3 with the N1 primer (Table 1) at the 5′ end of the Neo cassette amplified 3.4, 3.5, and 3.5 kb fragments, respectively (data not shown).

Screening of F1 heterozygotes—The correctly targeted ES cell lines from 129SvEv ES clones were microinjected into C57BL/6J blastocysts. The chimeric mice were crossbred with the C57BL/6J mice to generate germline transmission. The F1 heterozygotes were identified via PCR screening using the primer pairs A2/N1 and A3/N1 and then re-confirmed by primer pair A1/N1 with negative and positive controls (data not shown).

Establishment of Nmp4-KO-F2, Nmp4-WT-F2, and Nmp4-KO-N6 mice—The progeny of the mating of the first heterozygotes were a hybrid of 129SvEv and C57BL/6J. Both WT and Nmp4-KO mice in a 129SvEv and C57BL/6J F2 background were derived from the original heterozygous cross. In addition to the Nmp4-KO-F2 and Nmp4-WT-F2 mice we further backcrossed the KO mice onto a C57BL/6J background through six generations (Nmp4-KO-N6) and it were these mice that we have compared to C57BL/6J mice obtained from The Jackson Laboratories (Bar Harbor, ME) and used for the hormone studies. The genotypes of our mice were confirmed by two independent methods. Genomic DNA isolated from tail biopsies at weaning was evaluated by PCR analysis. The location of the primers for PCR (WT^1, WT^2, Neo^1, Neo^2, Table 1) are indicated in Figure 1A. Primers WT^1 and WT^2 amplify a 465 bp fragment and the Neo primers amplify a 512 bp fragment (see Fig. 1B). Additionally, Nmp4 expression in primary bone marrow-derived osteoblast cultures from WT and Nmp4-KO mice was compared using quantitative real-time PCR analysis (qRT-PCR) (see below for experimental details).

Dual energy X-ray absorptiometry (DEXA)

Areal bone mineral density (aBMD; mg/cm^2) and bone mineral content (BMC; g) were measured for the post-cranial skeleton by dual-energy X-ray absorptiometry (DEXA) using an X-ray pixiMUS mouse densitometer (PIXImus II; GE-Lunar Corp., Madison, WI). Mice were anesthetized with isoflurane (2% at 1.5 L/min) and placed in a prone position with limbs

outstretched on the pixiMUS platform. Body weight was recorded at this time. Growth rates were determined from the slopes of the weight×age regression lines.

Microcomputed tomography (μCT)

To assess trabecular micro architecture at the distal femoral metaphysis, the distal 25% of each femur was scanned on a desktop microcomputed tomographer (μCT 20, Scanco Medical AG, Bassersdorf, Switzerland) at 9 μm resolution. A microfocus X-ray tube with a focal spot of 10 μm was used as a source. For each slice, 600 projections were taken over 216° (180° plus half of the fan angle on either side). Precisely 205 microtomograph slices were acquired per bone using a slice increment of 17 μm. Distal femur stacks were reconstructed to the 3rd dimension using a standard convolution-backprojection procedure with a Shepp–Logan filter using a threshold value of 270. From the 3D constructs, trabecular bone volume per total volume (BV/TV), trabecular thickness (Tb Th), spacing (Tb Sp), and number (Tb N), connectivity density (Conn D), and structure model index (SMI) were calculated using the Scanco software. To assess cortical architecture, a single slice was taken through the midshaft femur, and the total area (TA), cortical area (CA), and second moments of inertia (I) were calculated from each midshaft slice.

PTH treatment regimen

Prior to the start of an experiment (8 weeks of age), mice, female WT and Nmp4-KO mice were given 0.01 ml sterile saline by subcutaneous (sc) injection once daily to acclimatize them to handling. At 10 weeks of age, mice were sorted into four groups of 11–12 mice each based on equivalent mean-group-body weight and were injected with human PTH 1-34 (Bachem Bioscience, Inc., Torrance, CA) at 30 μg/kg/day s.c., daily or vehicle control (0.2% BSA/0.1% 1.0 mN HCl in saline, Abbott Laboratory, North Chicago, IL) for 48 days and sacrificed on Day 49.

Primary bone marrow stromal cell (BMSC) culture

The muscle and connective tissue were removed from femurs and tibias of 6- to 8-week-old mice, the bones then briefly rinsed in 70% ethanol, and placed in PBS/HBSS at room temperature (Huang et al., 2004). The distal and proximal ends of the femurs and tibias were then cut and the marrow flushed with a tuberculin syringe, filled with complete α-MEM and cells, passage zero (P_0), were typically seeded at 3,000–6,000 cells/mm_2. On Day 5, the fresh medium was supplemented with 50 μg/ml of ascorbic acid and subsequently, the medium was replenished three times/week.

RNA extraction, cDNA synthesis, and quantitative real-time PCR (qRT-PCR) analysis

To harvest RNA from the femurs of 8-week-old female WT and Nmp4-null mice, freshly excised bones were transferred to liquid nitrogen and ground to a fine powder. The frozen bone powder was further homogenized in Trizol®(Invitrogen, Carlsbad, CA) using a Tissue-Tearor™(BioSpec Products, Inc., Bartlesville, OK). RNA was extracted from the Trizol-bone powder samples with chloroform and precipitated with isopropanol. The RNA pellet was further processed using the RNeasy Plus Mini Kit (QIAGEN, Inc., Valencia, CA). First strand cDNA synthesis was performed with First-Strand cDNA Synthesis Kit (Amersham Bioscience, Piscataway, NJ). Real-time PCR primers and probes were obtained from Assays-on-Demand™ (Applied Biosystems, Foster City, CA) for the following genes: alkaline phosphatase (Mm01187117_m1), COL1A1 (Mm00801666_g1), IGF-1 (Mm0043559_m1), MMP-13 (Mm00439491_m1) OPG (Mm00435452_m1), osteopontin (Mm00436767_m1), osterix (Mm00504574_m1), RANKL (Mm00441908_m1), and Runx2 (Mm00501578_m1). Custom design primer/probes were prepared for osteocalcin and Nmp4, and neomycin phospho transferase (Neo) (Table 1). We used the TaqMan Universal PCR Master Mix (Applied

Biosystems) for amplification in a Mastercycler ep realplex^2 real-time PCR system (Eppendorf, Westbury, NY). The qRT-PCR amplifications were performed in a sealed 96-well optical plate. The reaction conditions were as follows: 2 min at 50°C; 10 min at 95°C; 15 sec at 95°C; 1 min at 60°C; 40 cycles of 15 sec at 95°C, and 1 min at 60°C. Prior to assessing differences between WT and KO target gene expression we evaluated our experimental preparations for candidate normalizing genes using the Taqman Mouse Endogenous Control Array (Applied Biosystems) and choose RPLP2 (Mm03059047_gH). Samples that had equivalent levels of RPLP2 RNA expression were chosen for analysis. The ΔΔCT method was used to evaluate gene expression between WT and KO animals and the data represent the mean±standard deviation from at least six mice per genotype. Finally, BMSCs were seeded into 12-well culture dishes and at the indicated days post-seeding total cellular RNA was harvested from at least 6 independent cell cultures per genotype for qRT-PCR analysis. We determined that both RPLP2 and GAPDH were suitable as normalizing genes for these samples.

Statistical analyses

Statistical analysis was computed using JMP Version 7.0.1 (SAS Institute, Cary, NC). Typically, we used a two-factor ANOVA to determine if genotype and age, or genotype and treatment had a significant effect on a particular phenotypic parameter as well as to determine if interaction occurred between the independent variables of gene×age or gene×treatment. If the two-factor ANOVA indicated a significant effect for any of the independent variables, the data were then analyzed with a one-factor ANOVA followed by a Tukey's HSD post hoc test to determine significant differences between experimental groups. For some experiments, unpaired *t*-tests were employed as indicated. Genotype frequencies among mouse pups generated from heterozygous parents were tested for deviation from Mendelian ratios using the Chi-square test for goodness-of-fit. Data are presented as mean±SD. Statistical significance was taken at $P<0.05$.

Results

Targeted deletion of Nmp4/CIZ results in viable Nmp4-KO mice

Homologous recombination was used to replace exons 4–7 with the Neo gene cassette and the F1 heterozygotes were identified as described in Materials and Methods Section (Fig. 1A). The correct recombination event was confirmed both by PCR analysis of mouse tail DNA (Fig. 1B) and by analysis of Nmp4 expression in primary BMSC-derived osteoblasts (Fig. 1C). Animals homozygous for the Nmp4 deletion allele lacked any detectable Nmp4 mRNA in primary osteoblasts derived from bone marrow stromal cells (Fig. 1C), additionally, no Nmp4mRNA was detected in the femurs of Nmp4-KO mice (data not shown). Like the CIZ-deficient mice (Nakamoto et al., 2004;Morinobu et al., 2005), our Nmp4-KO mice appeared to be indistinguishable from WT littermates, were viable to adulthood, and showed no gross skeletal abnormalities (Fig. 1D). There was no significant difference in femur length at 8 weeks (WT=14.30±0.20 mm; KO=14.17±0.40 mm) and 17 weeks (WT=15.35±0.20 mm; KO=15.20 ±0.40 mm) of age between the Nmp4-KO-N6 and WTC57 BL/6J mice. In the process of backcrossing the Nmp4-KO genotype onto the C57BL/6J background we observed that matings between heterozygous (HZ Nmp4$^{+/-}$) mice produced a 1.4:2.1:0.5 genotype ratio among pups, which was found to deviate significantly from the 1:2:1 expected Mendelian frequencies ($\chi^2 = 6.1$, $P<0.05$). The diminished yield of KO pups from the predicted Mendelian ratios suggests that some of the KO embryos die either prior to birth or immediately after birth and we are presently investigating this phenomenon. Additionally, we observed that the size of the litters from Nmp4-KO-F2 crosses were modestly smaller than the litters from Nmp4-WT-F2 crosses of mice (pups/WT litters$_{9\ litters}$=7.4±1.4; pups/KO litters$_{10\ litters}$=5.4±2.6, average±SD; Prob> |*t*| 0.051). These observations are consistent with the sporadic infertility observed in CIZ-deficient mice due to spermatogenic cell degeneration (Nakamoto et al.,

2004). Finally, Nmp4-KO-F2 and Nmp4-WT-F2 litters produced on average an equal number of males and females (% males:% females/litter:WT 52.8±23.4:47.2±23.4; KO 44.6±19.8: 55.4 ±19.8; average±SD).

Nmp4/CIZ regulates basal bone mineral density, bone mineral content, and body weight

We observed a modest enhancement of baseline BMD and BMC in the Nmp4 KO mice as measured by DEXA. At 8 weeks of age the Nmp4-KO-N6 skeleton exhibited an approximate 8% increase in BMD in the whole body (WB) skeleton ($P<0.05$), tibia ($P<0.05$), and spine compared to the same bones of the WT mice (see Fig. 2A,C,G) whereas the difference in the femur BMD between these mice was less pronounced (Fig. 2E). Similarly, the Nmp4-N6-KO WB skeleton, tibia, spine and femur exhibited on average an approximate 10% enhancement in BMC as compared to their WT counterparts but these differences were not statistically significant (Fig. 2B,D,F,H). These trends were generally maintained at 16 weeks of age and the enhanced femur and spine BMCs achieved statistical significance (Fig. 2). Similarly, the Nmp4- KO-F2 mice exhibited a statistically significant 4% enhancement in WB BMD ($P<0.05$) and on average a 4% increase in WB BMC between 8 and 13 weeks (data not shown).

Consistent with the small increase in BMD and BMC we observed a modest, near significant enhancement of COL1A1 mRNA expression in the 8-week-old Nmp4-null femurs compared to WT bone using qRT-PCR (Fig. 3). However, no differences in the femur expression of Runx2, osterix, alkaline phosphatase IGF-1, MMP-13, OPG, osteocalcin, osteopontin, or RANKL were detected between WT and KO mice (data not shown). Bone marrow stromal cells from Nmp4-null and WT mice cultured under standard osteogenic conditions for 10–14 days (Huang et al., 2004) showed no difference in basal expression of these genes (data not shown).

The Nmp4 mutant alleles on a pure B6 background yielded a significant, 15% increase in body weight among the KO mice, compared to their WT controls (Fig. 4). Additionally, PIXImus analysis revealed no significant difference in percent body fat between WT and Nmp4-null mice (data not shown). Interestingly, the Nmp4-null mice prepared in a *129SvEv×C57BL/6 F2* background exhibited a significant 4% decrease in body weight as compared to the Nmp4-WT-F2 controls between 8 and 13 weeks of age as well as a modest but significant 2.5% decrease in percent body fat ($P<0.05$; data not shown). This is similar to the previous observation that CIZ-deficient mice prepared in a *DBA×C57BL/6 F2* background exhibited an approximately 10% decrease in body weight as compared to the CIZ-WT-F2 mice at 8 weeks of age (Morinobu et al., 2005). The opposing effects of Nmp4 mutation on body weight in the null-N6 and -F2 mice suggest the existence of a modifier gene(s) influencing this aspect of the mutant phenotype.

PTH induces a similar increase in skeletal BMD, BMC, and growth in WT and Nmp4-null mice

To evaluate the influence of Nmp4 on the skeletal response to anabolic doses of human PTH, WT and Nmp4-KO mice were injected daily with PTH or vehicle for 7 weeks. Intermittent doses of PTH had a similar effect on DXA-derived skeletal BMD and BMC in both genotypes, enhancing WB, femur, spine, and tibia BMD and BMC by two- to threefold over vehicle-treated mice in both the WT and Nmp4-null groups (Fig. 5A–H). While the PTH regimen was effective in building bone among both genotypes, we were unable to detect any significant differences between WT and Nmp4 null in responsiveness to PTH using DXA-derived measurements.

Hormone treatment modestly enhanced the growth rates (body weight gain from 10 to 17 weeks) of both the WT and Nmp4-KO mice, but the impact of PTH on weight gain was dramatically less than that observed for bone gain (Fig. 6). The Nmp4-KO mice gained

significantly less body mass during the treatment period than their WT counterparts, regardless of treatment, but hormone did not affect weight gain differently within the two genotypes (i.e., no significant interaction term was found).

Nmp4-KO mice exhibit an enhanced PTH-induced acquisition of trabecular bone compared to WT mice

PTH had a more dramatic impact on enhancing trabecular microarchitecture of the distal metaphyseal femur in the Nmp4-KO mice as compared to the WT mice (Fig. 7A–F). We examined the trabecular parameters of BV/TV, Conn D, SMI, Tb N, Tb Th, and Tb Sp using μCT analysis as described in Materials and Methods Section. We observed both genotype and treatment effects, as well as a genotype×treatment interaction for BV/TV, Conn D, and SMI (Fig. 7A–C). WT and Nmp4-null mice under the vehicle-control regimen exhibited equivalent BV/TV, Conn D, and SMI. Although hormone treatment significantly altered these parameters in both types of mice the magnitude of PTH-induced changes in the Nmp4-null mice ranged from 2.3- to 3.5-fold greater than the changes observed in the WT animals (Fig. 7A–C). Similarly, both the vehicle-treated WT and Nmp4-KO mice exhibited equivalent Tb N and Tb Th indices but the Nmp4-null mice response to hormone was approximately 1.5-fold greater than that of the WT mice in regard to these parameters (Fig. 7D,E). Finally, the vehicle-treated KO mice exhibited a significantly smaller Tb Sp than the vehicle-treated WT animals but the observed PTH-induced decrease in Tb Sp was similar in magnitude in both genotypes (Fig. 7F). Typical μCT scans from each of the four treatment groups is shown in Figure 8.

Untreated Nmp4-null mice exhibit midshaft femur cortical bone properties similar to those of PTH-treated WT mice

Next we examined the cortical bone geometry of the midshaft femurs from our four experimental groups using μCT analysis. The maximum and polar moments of inertia (I_{MAX} and J) were statistically identical (see Fig. 9A) and revealed only a modest trend toward enhanced bending and torsional properties among the KO femurs when compared to the corresponding WT femurs. I_{MIN} values for the KO VEH and KO PTH experimental groups were significantly greater than those values obtained from the WT VEH and WT PTH groups, respectively ($P<0.05$). Hormone significantly enhanced these parameters in both WT and null mice (Fig. 9A), but did so similarly in both genotypes (i.e., no genotype×treatment interaction). CA and TA have very similar profiles to those of the moments of inertia data (Fig. 9B), but MA was not influenced by either genotype or treatment (data not shown). Hormone significantly enhanced CA in both the WT and null mice but only significantly increased TA in the WT mice (Fig. 9B). Strikingly, the values of I_{MAX}, I_{MIN}, J, CA, and TA for the PTH-treated WT mice were not significantly different from those values observed for the untreated mice harboring Nmp4-null alleles.

Discussion

Nmp4/CIZ was independently discovered as a PTH-responsive osteoblast nuclear matrix DNA-binding protein (Nmp4, Alvarez et al., 1998) and as a nucleocytoplasmic shuttling transcription factor that binds to $p130^{cas}$ in rodent fibroblasts (CIZ, Nakamoto et al., 2000). Although ubiquitously expressed, its activity appears to be particularly significant to skeletal homeostasis.

Nmp4/CIZ acts to moderately suppress the acquisition of bone during skeletal growth and maturation. We observed an 8% and 10% increase in BMD and BMC, respectively throughout the 8- and 16-week-old Nmp4-null skeleton and this is similar to the previous observation that 8-week-old CIZ-deficient mice exhibited an enhanced femoral radiopacity and 40% increase in femoral BV/TV (Morinobu et al., 2005). The enhanced acquisition of bone in CIZ-deficient

animals resulted from elevated bone formation and mineral apposition rates and not to any perceptible change in bone resorption parameters (Morinobu et al., 2005). This is consistent with our observation that the baseline expression of COL1A1 mRNA was modestly elevated in the femurs of Nmp4-KO mice as compared to their WT counterparts. Furthermore, we have previously demonstrated that Nmp4 binds to the regulatory elements of rat COL1A1 and that over-expression of Nmp4 suppresses COL1A1 expression in rat osteoblast-like cells (Alvarez et al., 1997, 1998; Thunyakitpisal et al., 2001). Nevertheless, basal expression of selected genes supporting bone cell phenotype is indistinguishable in cultures of WT and Nmp4-KO mature osteoblasts. Whether there are differences in gene expression profiles between WT and Nmp4-null bone cells at earlier or later stages of differentiation is currently under investigation.

The additional effect of Nmp4/CIZ on body weight raises the question as to whether it plays a role in regulating the lineage fate of mesenchymal stem cells. Although both the F2- and N6-null mice exhibited an increase in BMD and BMC, this was not the case for body weight and percent body fat, suggesting that modifier genes influence Nmp4/CIZ regulation of some aspects of body composition. The Nmp4-KO-F2 mice exhibited a modest (4%) but significant decrease in body weight similar to that reported for the CIZ-KO-F2 mice (Morinobu et al., 2005). Our Nmp4-KO-F2 mice also showed a small but significant 2.5% reduction in percent body fat. This increase in bone and decrease in fat in the F2-null mice is consistent with the putative inverse relationship between the commitment of bone marrow-derived mesenchymal stem cells to the adipocyte and osteoblast lineage pathways (Gimble et al., 2006 and references therein). However our Nmp4-KO-N6 mice were on average 15% heavier than the WT counterparts but exhibited no difference in percent body fat suggesting an uncoupling of Nmp4/CIZ action on adipogenesis and osteogenesis in the pure B6 background. We are presently conducting a more comprehensive investigation on Nmp4/CIZ regulation of body composition.

The most profound impact of the loss-of-function Nmp4 mutation in our mice is the enhanced PTH-induced acquisition of trabecular bone without significantly influencing hormone-stimulated gains in cortical bone. The microarchitecture of the distal femur trabecular compartments of the vehicle-treated Nmp4-KO and WT mice at 17 weeks of age were identical as measured by BV/TV, Conn D, SMI, Tb N, and Tb Th but the PTH-induced changes in these parameters were between 1.5- and 3.5-fold greater in the Nmp4-null mice. In other words, the removal of Nmp4-KO facilitated greater PTH-induced trabecular bone gain. However, the impact of anabolic PTH on skeletal BMD and BMC were similar in both Nmp4-null and WT mice, which was comparable to the hormone response of WT C57BL/6 mice described in a previous study (Iida-Klein et al., 2002). Additionally, PTH-induced increases in the cortical area of the midshaft femur were not significantly different in the Nmp4-KO and WT mice suggesting that Nmp4/CIZ is critical for attenuating hormone-mediated gains in cancellous bone but does not actively suppress PTH-stimulated gains in all skeletal compartments including cortical bone. This is not surprising since the osteoblast and osteoclast responses to PTH are influenced by the apparent distinct microenvironments of cancellous and cortical bone. For example, transgenic mice expressing a constitutively active parathyroid hormone/parathyroid hormone-related protein receptor in osteoblast cells exhibited a significant increase in trabecular bone volume and a decrease in cortical thickness (Calvi et al., 2001). Similarly, PTH-stimulated periosteal bone formation was twofold higher in estrogen-replete female beta-arrestin2-null mice as compared to their WT counterparts, but the hormone response of the femoral and vertebral cancellous compartments were not as appreciably different in these two mice (Bouxsein et al., 2005).

Our previous in vitro studies suggest that Nmp4/CIZ suppresses PTH-induced gains in bone by acting as a transcriptional attenuator (Thunyakitpisal et al., 2001; Shah et al., 2004). Over-expression of Nmp4/CIZ in UMR-106-01 rat osteoblast-like cells not only suppresses basal COL1A1 transcription (Thunyakitpisal et al., 2001) but also PTH induction of MMP-13 (Shah

et al., 2004). There are conserved Nmp4/CIZ cis-elements in the human, rat, and mouse PTH response region of the MMP-13 gene (Bidwell et al., 2001; Shah et al., 2004). In an earlier study, we prepared a series of promoter–reporter constructs of the MMP-13 gene containing the first 1,329 nucleotides of the 5′-regulatory region and introduced null-binding mutations in the Nmp4/CIZ element and/or the proximal Runx2 cis-element (Shah et al., 2004). The activity of the WT MMP-13 construct increased by twofold when challenged with rat PTH (1–34) for 6 h in UMR-106-01 rat osteoblast-like cells. However, the promoter–reporter construct harboring a null-binding mutation in the Nmp4/CIZ site responded to hormone stimulation with a significantly enhanced fivefold increase in activity. Finally, mutation of a proximal Runx2 site within this PTH region slightly attenuated the PTH response, however, mutation of this site and the Nmp4/CIZ element together resulted in an 11-fold increase in PTH-induced activity (Shah et al., 2004). Therefore, as a trans-acting protein Nmp4/CIZ attenuates the magnitude of the transcriptional response to PTH and its proximity to Runx2 may enhance this function. Furthermore, CIZ over-expression suppressed BMP2-induced Runx2 promoter activity in MC3T3-E1 osteoblast-like cells (Shen et al., 2002) thus Nmp4/CIZ may govern the action of Runx2 not only by interfering with its activity along the regulatory regions of PTH target genes, but also by attenuating its expression, although we did not observed an enhanced baseline expression of Runx2 in the femurs of our Nmp4-KO mice or from osteoblasts derived from these bones. Consistent with our hypothesis that the Nmp4/CIZ pathway may be linked to an endocrine feedback circuit, we have reported that PTH attenuated the activities of the mouse Nmp4 P_1 and P_2 promoters in MC3T3-E1 osteoblasts (Alvarez et al., 2005) thus providing a potential means for the hormone to regulate its own regulator. Nevertheless further studies are required to elucidate the cellular and molecular events responsible for the enhanced response to anabolic doses of PTH in the Nmp4-null mice.

Disabling Nmp4/CIZ appears to enhance anabolic gains in bone and neutralize catabolic bone loss. As previously mentioned CIZ attenuates BMP2-mediated increases in osteoblast gene expression in vitro (Shen et al., 2002) and bone formation in vivo (Morinobu et al., 2005) and the mutations in the MMP-13 Nmp4/CIZ cis-element described above also enhance this gene's response to prostaglandin E2 (Shah et al., 2004). Remarkably CIZ deficiency also abrogates unloading-induced bone loss (Hino et al., 2007). Those data suggest that Nmp4/CIZ might constitutively suppress osteoid synthesis and neutralizing its action allows matrix production under typically catabolic conditions. The suppressive action of Nmp4/CIZ on osteoid synthesis may be particularly sensitive to changes in the mechanical environment of the osteoblast since both PTH and load have a physical impact on bone cells (Egan et al., 1991; Horikawa et al., 2000) and these agonists activate some of the same signaling pathways in bone cells (Ryder and Duncan, 2001; Zhang et al., 2006). Consistent with the absence of bone loss in unloaded CIZ-deficient mice, Nmp4/CIZ contributes to fluid shear stress-induced changes in MMP-13 expression in MC3T3-E1 cells via the PTH response region of this gene (Charoonpatrapong-Panyayong et al., 2007).

Nmp4/CIZ has been put forward as a potential drug target for the treatment of osteoporosis (Krane, 2005) and the present data strengthen this proposition. Furthermore, its presence in the cytoplasm may make it a more accessible target than the typical transcription factor. In the present study hormone treatment caused a significant decrease in SMI in both the WT and KO mice, indicating that PTH altered trabecular architecture from a rod-like to a plate-like morphology, consistent with an increase in bone strength. Nevertheless, this decrease in SMI was significantly exaggerated in the KO mice (3.5-fold). Additionally, our untreated Nmp4-KO mice exhibited similar bone mass and geometric properties as the PTH-treated WT mice suggesting that therapies designed to inhibit Nmp4/CIZ might yield similar benefits to bone mass and strength as those achieved via daily PTH administration.

Acknowledgments

Contract grant sponsor: NIH NIDDK;

Contract grant number: DK053796.

This work was supported by a grant from NIH NIDDK, contract grant number: DK053796 (to JPB). We thank Marta Alvarez and Rita Shah for their technical assistance.

Literature Cited

Alvarez M, Long H, Onyia J, Hock J, Xu W, Bidwell J. Rat osteoblast and osteosarcoma nuclear matrix proteins bind with sequence specificity to the rat type I collagen promoter. Endocrinology 1997;138:482–489. [PubMed: 8977438]

Alvarez M, Thunyakitpisal P, Morrison P, Onyia J, Hock J, Bidwell JP. PTH-responsive osteoblast nuclear matrix architectural transcription factor binds to the rat type I collagen promoter. J Cell Biochem 1998;69:336–352. [PubMed: 9581872]

Alvarez M, Shah R, Rhodes SJ, Bidwell JP. Two promoters control the mouse Nmp4/CIZ transcription factor gene. Gene 2005;347:43–54. [PubMed: 15716059]

Bellido T, Ali AA, Plotkin LI, Fu Q, Gubrij I, Roberson PK, Weinstein RS, O'Brien CA, Manolagas SC, Jilka RL. Proteasomal degradation of Runx2 shortens parathyroid hormone-induced anti-apoptotic signaling in osteoblasts. A putative explanation for why intermittent administration is needed for bone anabolism. J Biol Chem 2003;278:50259–50272. [PubMed: 14523023]

Bidwell JP, Torrungruang K, Alvarez M, Rhodes SJ, Shah R, Jones DR, Charoonpatrapong K, Hock JM, Watt AJ. Involvement of the nuclear matrix in the control of skeletal genes: The NMP1 (YY1), NMP2 (Cbfa1), and NMP4 (Nmp4/CIZ) transcription factors. Crit Rev Eukaryot Gene Expr 2001;11:279–297. [PubMed: 12067068]

Bikle DD, Sakata T, Leary C, Elalieh H, Ginzinger D, Rosen CJ, Beamer W, Majumdar S, Halloran BP. Insulin-like growth factor I is required for the anabolic actions of parathyroid hormone on mouse bone. J Bone Miner Res 2002;17:1570–1578. [PubMed: 12211426]

Bouxsein ML, Pierroz DD, Glatt V, Goddard DS, Cavat F, Rizzoli R, Ferrari SL. Beta-Arrestin2 regulates the differential response of cortical and trabecular bone to intermittent PTH in female mice. J Bone Miner Res 2005;20:635–643. [PubMed: 15765183]

Calvi LM, Sims NA, Hunzelman JL, Knight MC, Giovannetti A, Saxton JM, Kronenberg HM, Baron R, Schipani E. Activated parathyroid hormone/parathyroid hormone-related protein receptor in osteoblastic cells differentially affects cortical and trabecular bone. J Clin Invest 2001;107:277–286. [PubMed: 11160151]

Charoonpatrapong-Panyayong K, Shah R, Yang J, Alvarez M, Pavalko FM, Gerard-O'Riley R, Robling AG, Templeton E, Bidwell JP. Nmp4/CIZ contributes to fluid shear stress induced MMP-13 gene induction in osteoblasts. J Cell Biochem 2007;102:1202–1213. [PubMed: 17455210]

Dempster DW, Cosman F, Kurland ES, Zhou H, Nieves J, Woelfert L, Shane E, Plavetic K, Muller R, Bilezikian J, Lindsay R. Effects of daily treatment with parathyroid hormone on bone microarchitecture and turnover in patients with osteoporosis: A paired biopsy study. J Bone Miner Res 2001;16:1846–1853. [PubMed: 11585349]

Egan JJ, Gronowicz G, Rodan GA. Parathyroid hormone promotes the disassembly of cytoskeletal actin andmyosin in cultured osteoblastic cells: Mediation by cyclic AMP. J Cell Biochem 1991;45:101–111. [PubMed: 1848561]

Feister HA, Onyia JE, Miles RR, Yang X, Galvin R, Hock JM, Bidwell JP. The expression of the nuclear matrix proteins NuMA, topoisomerase II-alpha, and -beta in bone and osseous cell culture: Regulation by parathyroid hormone. Bone 2000;26:227–234. [PubMed: 10709994]

Gimble JM, Zvonic S, Floyd ZE, Kassem M, Nuttall ME. Playing with bone and fat. J Cell Biochem 2006;98:251–266. [PubMed: 16479589]

Hino K, Nakamoto T, Nifuji A, Morinobu M, Yamamoto H, Ezura Y, Noda M. Deficiency of CIZ, a nucleocytoplasmic shuttling protein, prevents unloading-induced bone loss through the enhancement of osteoblastic bone formation in vivo. Bone 2007;40:852–860. [PubMed: 17301008]

Horikawa A, Okada K, Sato K, Sato M. Morphological changes in osteoblastic cells (MC3T3-E1) due to fluid shear stress: Cellular damage by prolonged application of fluid shear stress. Tohoku J Exp Med 2000;2000:127–137. [PubMed: 10997553]

Huang JC, Sakata T, Pfleger LL, Bencsik M, Halloran BP, Bikle DD, Nissenson RA. PTH differentially regulates expression of RANKL and OPG. J Bone Miner Res 2004;19:235–244. [PubMed: 14969393]

Hurley MM, Okada Y, Xiao L, Tanaka Y, Ito M, Okimoto N, Nakamura T, Rosen CJ, Doetschman T, Coffin JD. Impaired bone anabolic response to parathyroid hormone in Fgf2−/− and Fgf2+/− mice. Biochem Biophys Res Commun 2006;341:989–994. [PubMed: 16455048]

Iida-Klein A, Zhou H, Lu SS, Levine LR, Ducayen-Knowles M, Dempster DW, Nieves J, Lindsay R. Anabolic action of parathyroid hormone is skeletal site specific at the tissue and cellular levels in mice. J Bone Miner Res 2002;17:808–816. [PubMed: 12009011]

Jilka RL. Molecular and cellular mechanisms of the anabolic effect of intermittent PTH. Bone 2007;40:1434–1446. [PubMed: 17517365]

Krane SM. Identifying genes that regulate bone remodeling as potential therapeutic targets. J Exp Med 2005;201:841–843. [PubMed: 15781576]

Leupin O, Kramer I, Collette NM, Loots GG, Natt F, Kneissel M, Keller H. Control of the SOST bone enhancer by PTH using MEF2 transcription factors. J Bone Miner Res 2007;22:1957–1967. [PubMed: 17696759]

Li X, Liu H, Qin L, Tamasi J, Bergenstock M, Shapses S, Feyen JH, Notterman DA, Partridge NC. Determination of dual effects of parathyroid hormone on skeletal gene expression in vivo by microarray and network analysis. J Biol Chem 2007;282:33086–33097. [PubMed: 17690103]

Liu F, Lee SK, Adams DJ, Gronowicz GA, Kream BE. CREM deficiency in mice alters the response of bone to intermittent parathyroid hormone treatment. Bone 2007;40:1135–1143. [PubMed: 17275432]

Martin TJ, Seeman E. New mechanisms and targets in the treatment of bone fragility. Clin Sci (Lond) 2007;112:77–91. [PubMed: 17155930]

Merciris D, Marty C, Collet C, de Vernejoul MC, Geoffroy V. Overexpression of the transcriptional factor Runx2 in osteoblasts abolishes the anabolic effect of parathyroid hormone in vivo. Am J Pathol 2007;170:1676–1685. [PubMed: 17456773]

Morinobu M, Nakamoto T, Hino K, Tsuji K, Shen ZJ, Nakashima K, Nifuji A, Yamamoto H, Hirai H, Noda M. The nucleocytoplasmic shuttling protein CIZ reduces adult bone mass by inhibiting bone morphogenetic protein-induced bone formation. J Exp Med 2005;201:961–970. [PubMed: 15781586]

Nakamoto T, Yamagata T, Sakai R, Ogawa S, Honda H, Ueno H, Hirano N, Yazaki Y, Hirai H. CIZ, a zinc finger protein that interacts with p130(cas) and activates the expression of matrix metalloproteinases. Mol Cell Biol 2000;20:1649–1658. [PubMed: 10669742]

Nakamoto T, Shiratsuchi A, Oda H, Inoue K, Matsumura T, Ichikawa M, Saito T, Seo S, Maki K, Asai T, Suzuki T, Hangaishi A, Yamagata T, Aizawa S, Noda M, Nakanishi Y, Hirai H. Impaired spermatogenesis and male fertility defects in CIZ/Nmp4-disrupted mice. Genes Cells 2004;9:575–589. [PubMed: 15189450]

Neer RM, Arnaud CD, Zanchetta JR, Prince R, Gaich GA, Reginster JY, Hodsman AB, Eriksen EF, Ish-Shalom S, Genant HK, Wang O, Mitlak BH. Effect of parathyroid hormone (1– 34) on fractures and bone mineral density in postmenopausal women with osteoporosis. N Engl J Med 2001;344:1434–1441. [PubMed: 11346808]

Ryder KD, Duncan RL. Parathyroid hormone enhances fluid shear-induced [Ca2+]i signaling in osteoblastic cells through activation of mechanosensitive and voltage-sensitive Ca2+ channels. J Bone Miner Res 2001;16:240–248. [PubMed: 11204424]

Shah R, Alvarez M, Jones DR, Torrungruang K, Watt AJ, Selvamurugan N, Partridge NC, Quinn CO, Pavalko FM, Rhodes SJ, Bidwell JP. Nmp4/CIZ regulation of matrix metalloproteinase 13 (MMP-13) response to parathyroid hormone in osteoblasts. Am J Physiol Endocrinol Metab 2004;287:E289–E296. [PubMed: 15026307]

Shen ZJ, Nakamoto T, Tsuji K, Nifuji A, Miyazono K, Komori T, Hirai H, Noda M. Negative regulation of bone morphogenetic protein/Smad signaling by Cas-interacting zinc finger protein in osteoblasts. J Biol Chem 2002;277:29840–29846. [PubMed: 12023967]

Swarthout JT, D'Alonzo RC, Selvamurugan N, Partridge NC. Parathyroid hormone-dependent signaling pathways regulating genes in bone cells. Gene 2002;282:1–17. [PubMed: 11814673]

Thunyakitpisal P, Alvarez M, Tokunaga K, Onyia JE, Hock J, Ohashi N, Feister H, Rhodes SJ, Bidwell JP. Cloning and functional analysis of a family of nuclear matrix transcription factors (NP/NMP4) that regulate type I collagen expression in osteoblasts. J Bone Miner Res 2001;16:10–23. [PubMed: 11149472]

Yakar S, Bouxsein ML, Canalis E, Sun H, Glatt V, Gundberg C, Cohen P, Hwang D, Boisclair Y, Leroith D, Rosen CJ. The ternary IGF complex influences postnatal bone acquisition and the skeletal response to intermittent parathyroid hormone. J Endocrinol 2006;189:289–299. [PubMed: 16648296]

Zhang J, Ryder KD, Bethel JA, Ramirez R, Duncan RL. PTH-induced actin depolymerization increases mechanosensitive channel activity to enhance mechanically stimulated Ca2+ signaling in osteoblasts. J Bone Miner Res 2006;21:1729–1737. [PubMed: 17002579]

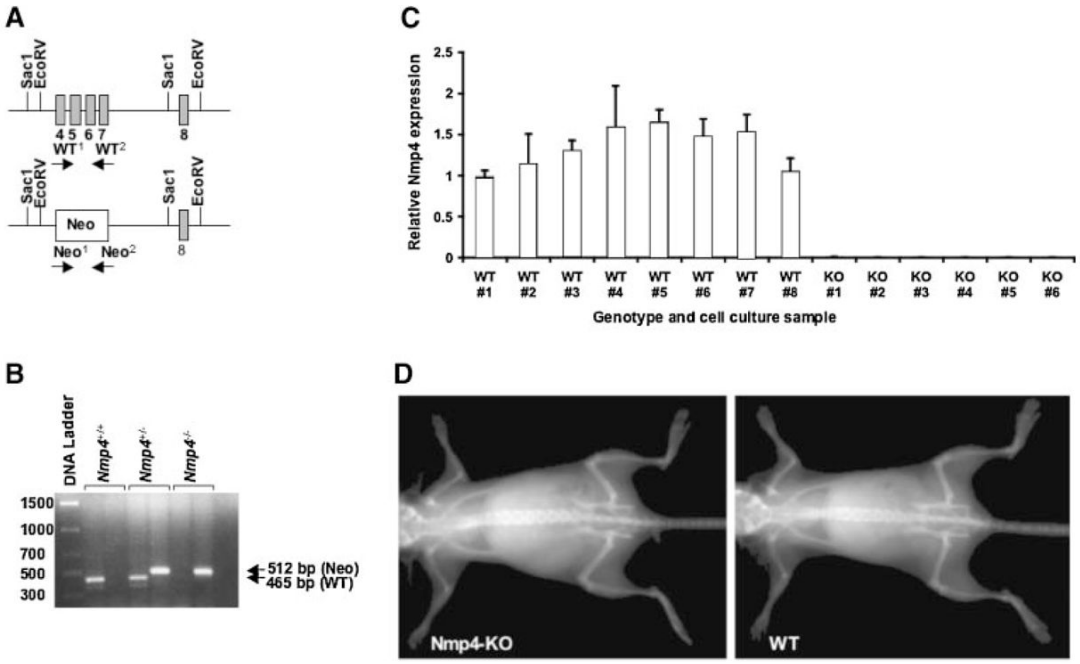

Fig. 1.

Nmp4-KO mice exhibit no Nmp4 expression but the gross appearance of the skeleton is indistinguishable from that of the WT mice. A: The gene-targeting strategy for KO mice involves replacing exons 4–7 with the Neo cassette. A partial restriction map of the Nmp4 gene is displayed. Shaded boxes indicate the numbered exons and thin lines represent the introns. The locations of PCR primers WT1, WT2, Neo1, Neo2 are indicated with arrows. B: PCR analysis of mouse tail DNA isolated from 21-day-old pups obtained from $Nmp4^{+/-}$ intercrosses. Primers WT^1 and WT^2 amplify a 465 bp fragment; primers Neo^1 and Neo^2 amplify a 512bp fragment indicating transmission of the targeted (KO) allele. The faint band below the main WT fragment is a predicted minor band within our target sequence. The presence of Neo is confirmed in heterozygous ($Nmp4^{+/-}$) and KO($Nmp4^{-/-}$) animals. C:Bone marrow stromal cells were obtained from the femurs of eight WT and six Nmp4-null (KO) mice and maintained in 12-well plates under ascorbic acid to enhance osteoblast differentiation. After 10–14 days in culture RNA was harvested and evaluated for relative Nmp4 expression (compared to WT #1) using qRT-PCR analysis as described in Materials and Methods Section. No Nmp4 transcripts were detected in cell cultures derived from Nmp4-KO mice similarly no Nmp4 transcripts were detected in mRNA from mouse bone (8 weeks old, data not shown). D: X-rays of 8-week-old female WT and Nmp4-null mice are indistinguishable.

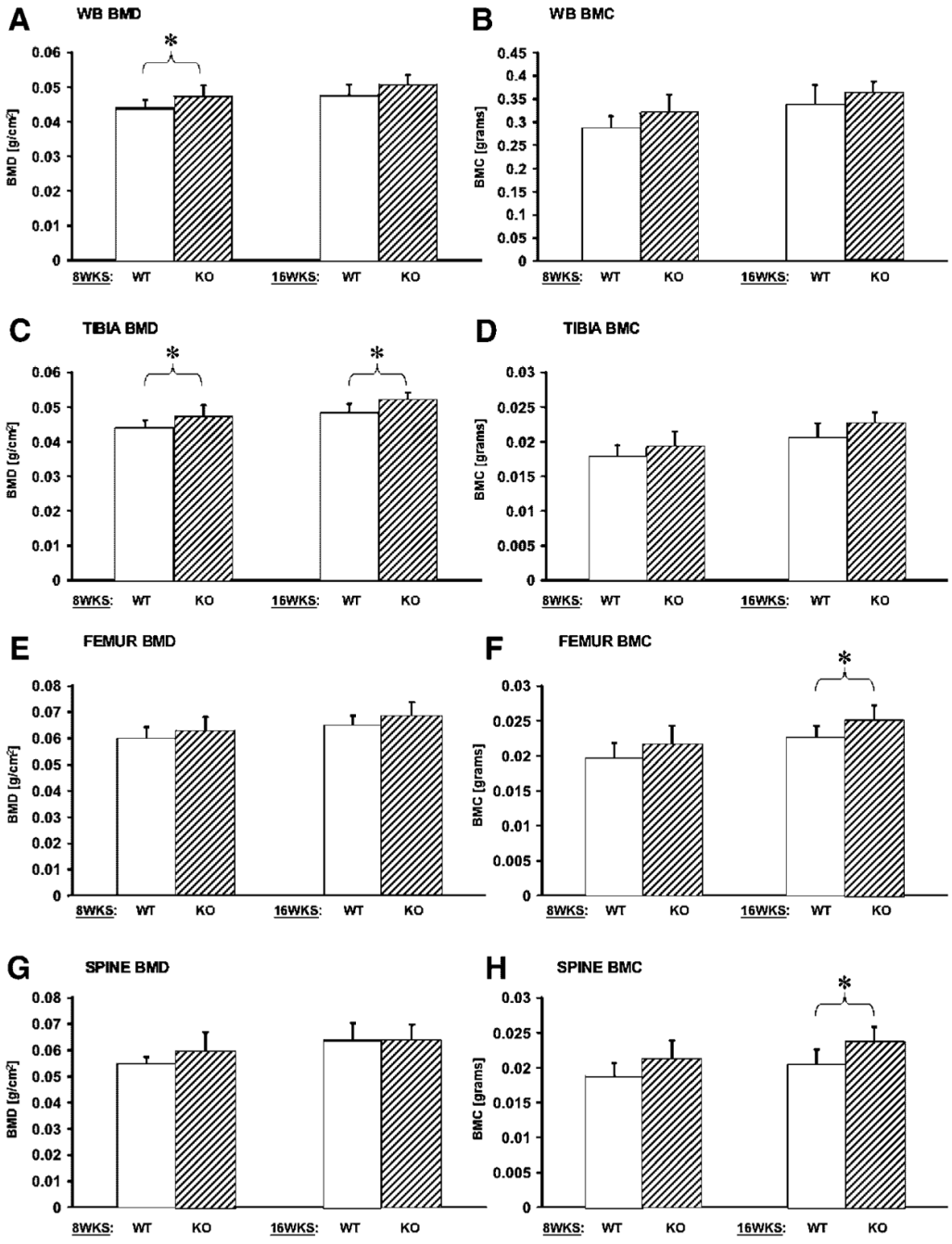

Fig. 2.

Nmp4-null mice typically exhibited an approximate 8% increase in BMD and 10% increase in BMC compared to WT animals at both 8 and 16 weeks of age. PIXImus analyses of 8- and 16-week-old WT and Nmp4-KO mice (n=10–12 mice/group) for (A) whole body (WB) BMD, (B) WB BMC; (C) tibia BMD, (D) tibia BMC; (E) femur BMD, (F) femur BMC; (G) spine BMD; (H) spine BMC. Data were analyzed with a two-way ANOVA using genotype and age as independent variables, followed by a one-way ANOVA and Tukey's HSD test comparing experimental groups (average±SD; asterisk indicates $P < 0.05$).

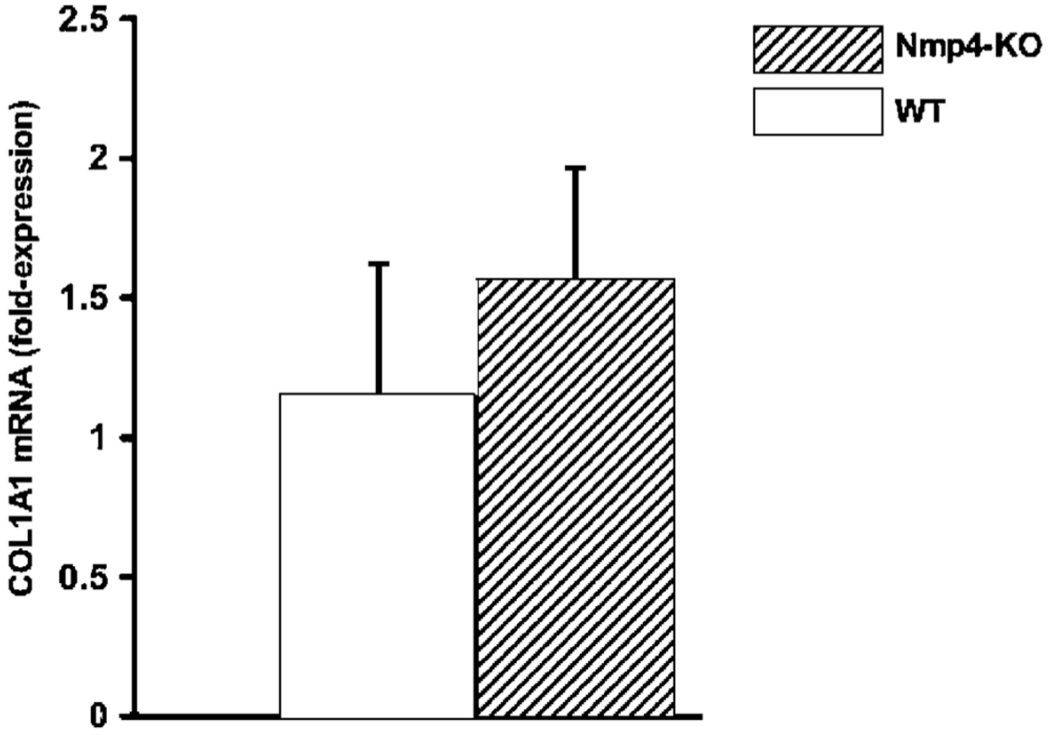

Fig. 3.

Nmp4-null mice exhibited a modestly enhanced expression of COL1A1 mRNA. Total RNA was extracted from femurs of 8-week-old female Nmp4-null and WT mice (n=6–8/genotype) and analyzed using qRT-PCR as described in Materials and Methods Section. Data were analyzed with a *t*-test (average±SD; Prob > |*t*| 0.0781).

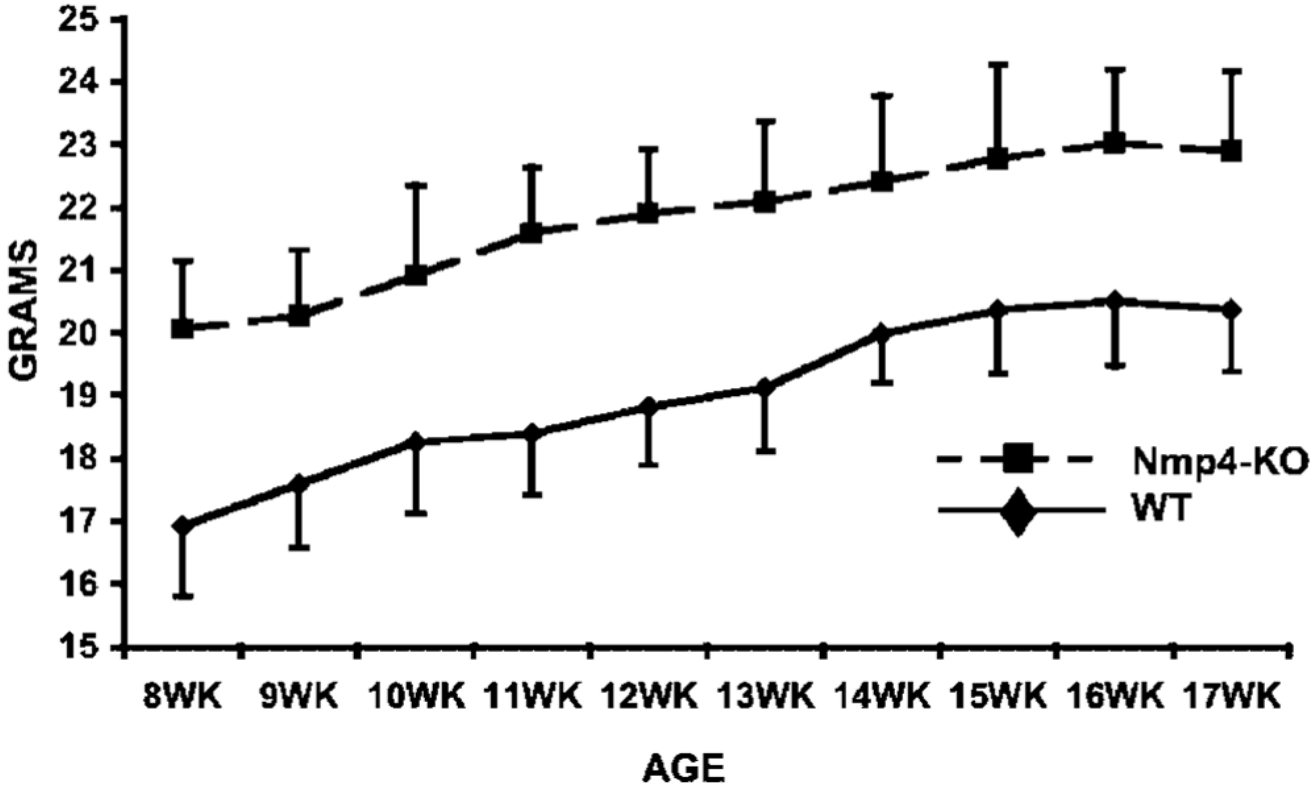

Fig. 4.

Nmp4-KO-N6 (n=11) mice exhibit a 15% increase in body weight as compared to their WT counterparts over 8–17 weeks of age (n=12, average±SD, $P < 0.05$).

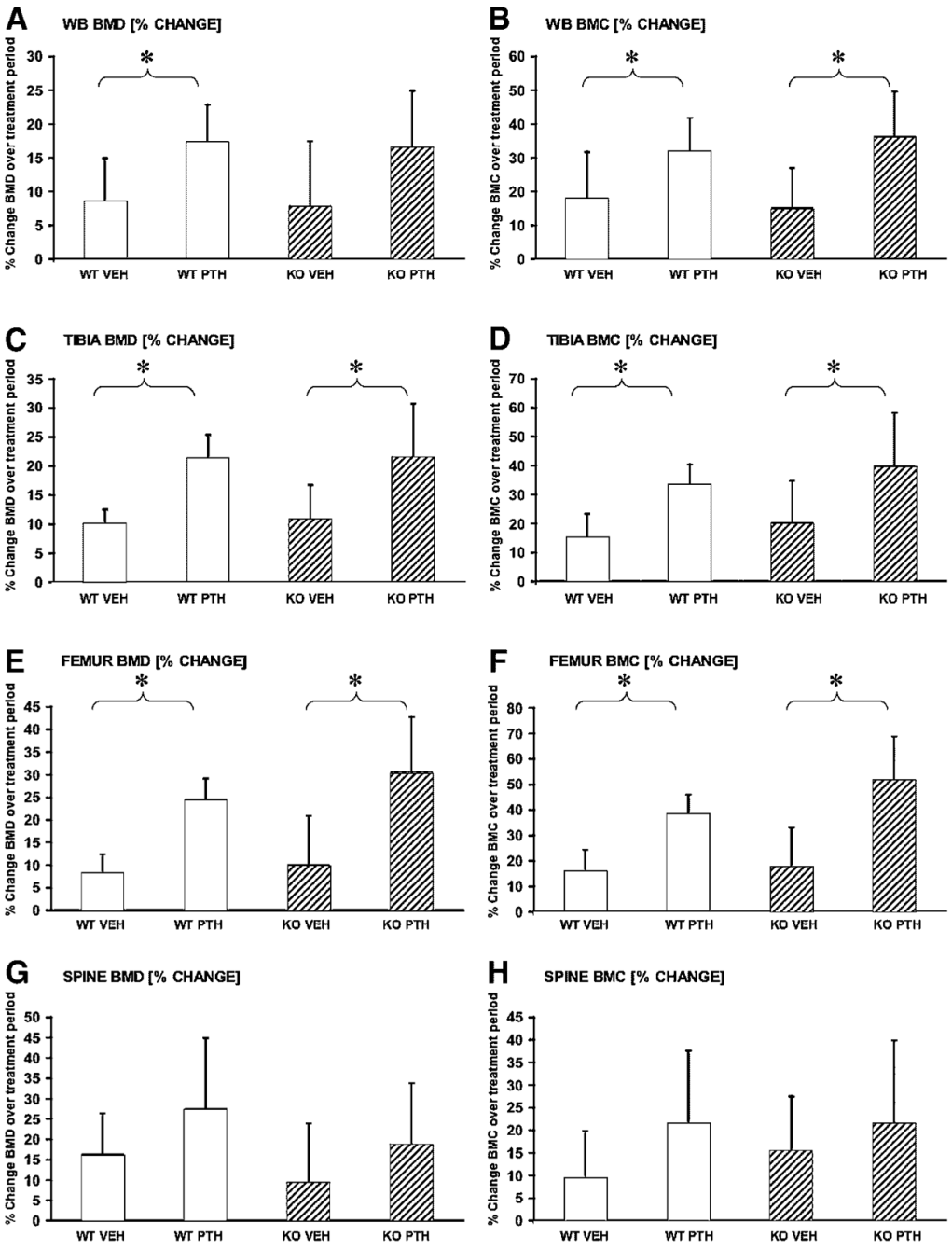

Fig. 5.

PTH induces a similar increase in skeletal BMD and BMC in WT and Nmp4-nullmice. Mice were sorted into four experimental groups (WT treated with vehicle [VEH] n=12, WT treated with hormone [PTH] n=12, Nmp4-KO-N6 [KO] treated with VEH n=11, and KO treated with PTH, n=11). DEXA measurements were obtained on each mouse at 8 and 17 weeks of age and the percent change determined. Hormone treatment significantly enhanced WB, femur, and tibia BMD and BMC by two-to threefold over vehicle-treated mice in both the WT and Nmp4-null groups (average±SD; asterisk indicates $P < 0.05$). PTH treatment enhanced spine BMD and BMC in both WT and Nmp4-KO mice but the effect of hormone on these skeletal parameters was not statistically significant.

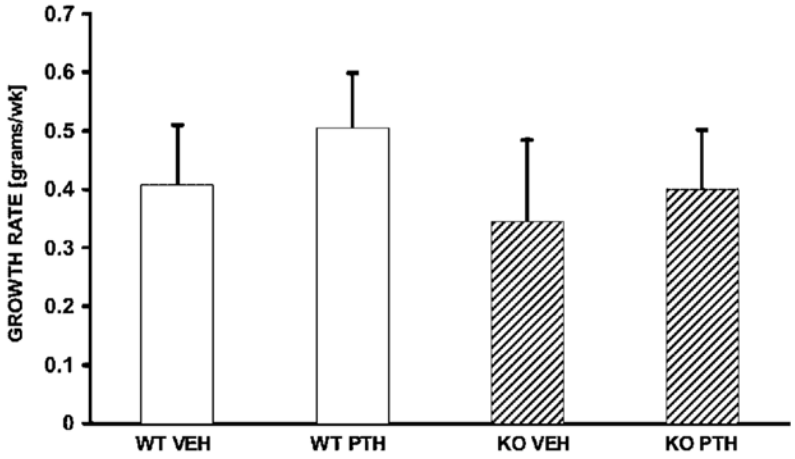

Fig. 6.

The Nmp4-KO mice gained significantly less body mass during the treatment period than their WT counterparts, regardless of treatment, and although PTH enhanced body mass in both WT and KO mice hormone did not affect weight gain differently within the two genotypes (two-way ANOVA: Genotype Prob > |*t*| 0.0138; Treatment Prob > |*t*| 0.0234; Genotype×Treatment Prob > |*t*| 0.5229). Growth rates were estimated as described in Materials and Methods Section.

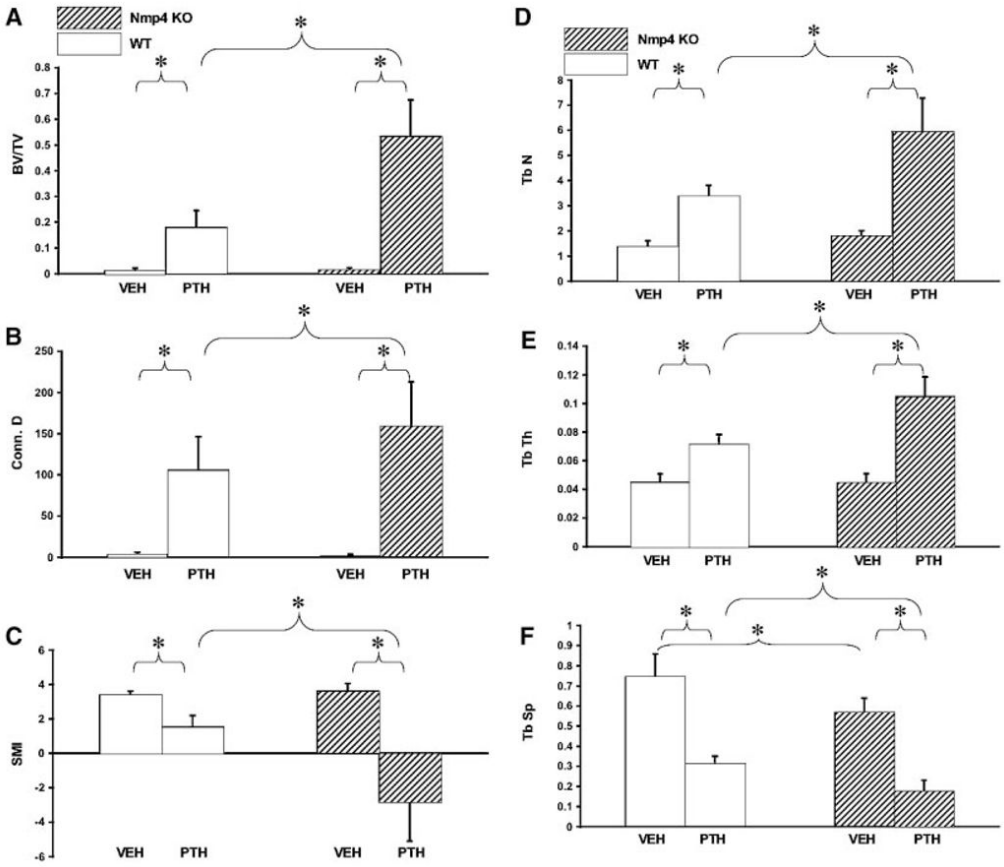

Fig. 7.

PTH had a more dramatic impact on enhancing trabecular microarchitecture of the distal metaphyseal femur in the Nmp4-KO-N6 mice as compared to the WT C57BL/6J mice. Mouse femurs from the four treatment groups (WT VEH, n=12; WT PTH, n=12; KO VEH, n=8; KO PTH, n=9) were analyzed using μCT as described in Materials and Methods Section. Parameters include (A) BV/TV=bone volume/total volume; (B) Conn D=connectivity density; (C) SMI=structural model index; (D) TbN=trabecular number; (E) Tb Th=trabecular thickness; (F) Tb Sp=trabecular spacing; (average±SD, asterisk indicates $P < 0.05$, note two-way ANOVA shows a strong genotype×treatment interaction for all parameters except Tb Sp).

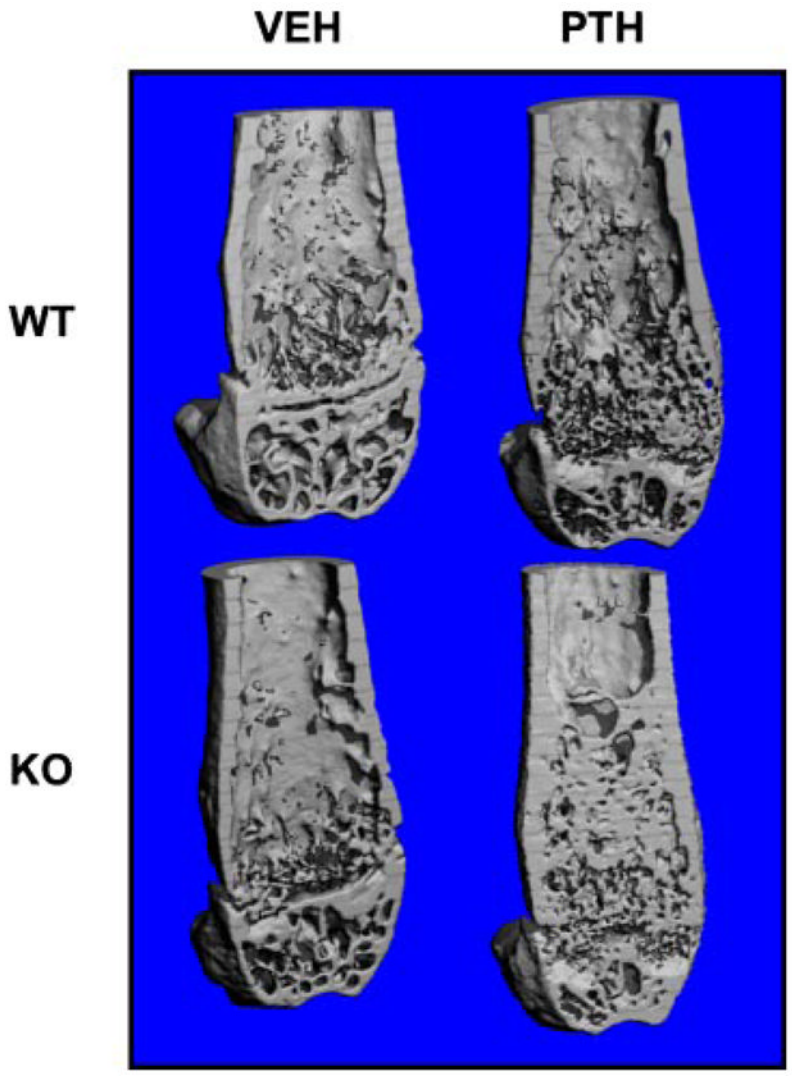

Fig. 8.

Typical μCT scans from the four experimental treatment groups visually demonstrate the enhanced PTH-induced trabecular architecture in the Nmp4-nullmice. Images of the distal metaphyseal femur, acquired as described in Materials and Methods Section, were obtained from mice at the end of the 49-day treatment period and include WT treated with vehicle (VEH); WT treated with PTH; KO treated with VEH; KO treated with PTH. [Color figure can be viewed in the online issue, which is available at www.interscience.wiley.com.]

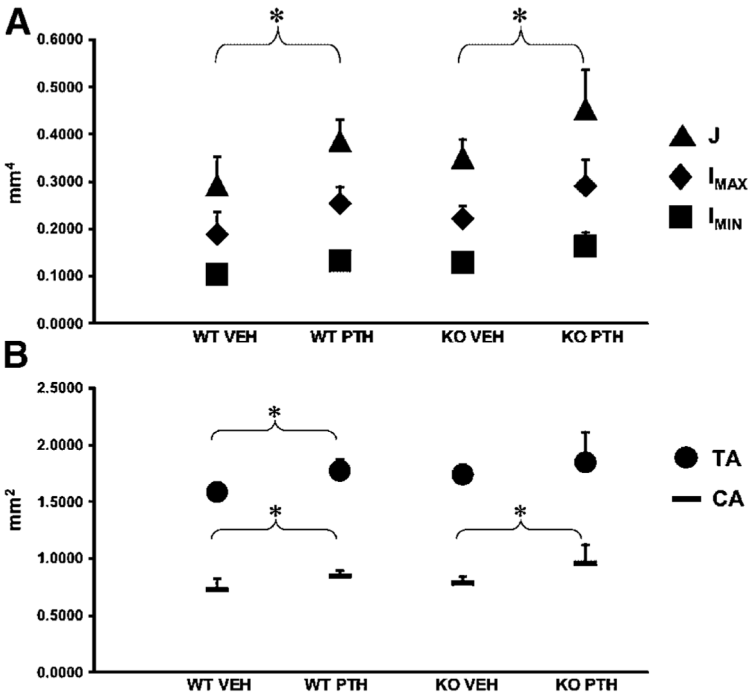

Fig. 9.

Untreated Nmp4-KO mice exhibited similar cortical bone geometry properties as those of the PTH-treated WT mice. Mouse femurs from the four treatment groups (WTVEH, n=12;WT PTH, n=12; KOVEH, n=11; KOPTH, n=12) were analyzed using μCT as described in Materials and Methods Section. Parameters of the femoral midshaft cortical bone included (A) midshaft cross section maximum moment of inertia (I_{MAX}), minimum moment of inertia (I_{MIN}), and polar moment of inertia (J) and (B) cortical area (CA) and total area (TA). PTH significantly elevated nearly all geometric properties except for TA in the Nmp4-null mice (average±SD; asterisk indicates $P < 0.05$). There was no genotype×treatment interaction. Not indicated by an asterisk due to space limitations, the I_{MIN} values for the KOVEH and KOPTH experimental groups were significantly greater than those values obtained from the WTVEH and WT PTH groups, respectively ($P < 0.05$).

TABLE 1

Oligonucleotide primers used in PCR reactions

Primer	Sequence
Primers for screening recombinant clones and F1 heterozygotes	
NMPYA1	5′-GTGATATCAAGGTTAGTGGGAAGAC-3′
NMPYA2	5′-CTGAATGGTAGTAACGGCTCAGAG-3′
A1	5′-GAGAAAGACAGAGGTTATACTTGAC-3′
A2	5′-GATTCATGTCTAGGGGCATGTCTTC-3′
A3	5′-CTGGAGACTCATTCTGTAGACCAG-3′
Primers for genotyping tail biopsies	
N1	5′-TGCGAGGCCAGAGGCCACTTGTGTAGC-3′
WT[1]	5′-ACCCGTACTTCTGGCCTTCT-3′
WT[2]	5′-CTGAGGCAGGGACAGTTAGC-3′
Neo[1]	5′-AGGATCTCCTGTCATCTCACCTTGCTCCTG-3′
Neo[2]	5′-AAGAACTCGTCAAGAAGGCAATAGAAGGCG-3′
Custom ABI primers for evaluating gene expression	
Osteocalcin (forward)	5′-CTGACAAAGCCTTCATGTCCAA-3′
Osteocalcin (probe)	5′-AGGAGGGCAATAAGGTAGT-3′
Osteocalcin (reverse)	5′-GGTAGCGCCGGAGTCTGTT-3′
Nmp4 (forward)	5′-CACAGTCTCAGGGCAGATTGAA-3′
Nmp4 (probe)	5′-ACACTATGTTCATCAACAAG-3′
Nmp4 (reverse)	5′-CTCTGGCAACAGCTGATCCTT-3′
Neo (forward)	5′-AGATGGATTGCACGCAGGTT-3′
Neo (probe)	5′-TCCGGCCGCTTGG-3′
Neo (reverse)	5′-GCCCAGTCATAGCCGAATAGC-3′